4E analysis and multi-objective optimization of an integrated MCFC (molten carbonate fuel cell) and ORC (organic Rankine cycle) system

Alireza Haghighat Mamaghani [a], Behzad Najafi [a], Ali Shirazi [b,*], Fabio Rinaldi [a]

[a] Dipartimento di Energia, Politecnico di Milano, Via Lambruschini 4, 20156 Milano, Italy
[b] School of Mechanical and Manufacturing Engineering, The University of New South Wales (UNSW), Kensington, New South Wales 2052, Australia

Received 12 October 2014
Received in revised form
21 January 2015
Accepted 24 January 2015
Available online 20 February 2015

1. Introduction

The escalating fuel price, stricter environmental legislations, and continuous increase in energy consumption pose an urgent need for power generation technologies to operate in a more efficient, cost-effective and environment-friendly manner [1–3]. Furthermore, in the recent years, the distributed power generation has been identified as an economically viable option for small scale applications (up to several megawatts) and specifically for providing electrification to remote areas without access to public grid [4]. Within this context, fuel cells, especially MCFC (molten carbonate fuel cell) and SOFC (solid oxide fuel cell) have come into sight as competent alternatives to conventional power generation methods [5]. MCFC as a typical high-temperature fuel cell has attracted a great deal of attention due to its high efficiency, low emission of pollutants, and fuel flexibility based on its resistance to fuel impurities such as CO (carbon monoxide) [6]. Moreover, operation at elevated temperatures (600–700 °C) entails sufficient fast kinetics, allowing MCFC to use relatively inexpensive non-noble catalysts (Ni vs. Pt) [7]. In addition, one of the most encouraging characteristics of high temperature fuel cells, such as MCFC, is the high temperature of the exhaust gas, offering the possibility of cogeneration purposes or combination with other types of power generators such as gas turbine [8,9] and organic Rankine cycle (ORC) [10] to achieve a high efficiency and provide additional power.

Beside the experimental studies [5,11], many modeling and simulation studies of the MCFC have been going on to examine the electrochemical processes, the transport phenomena, and cell design [12–14]. A good overview over some steady-state models of MCFCs can be found in Koh et al. [15]. Likewise, in the development of integrated power systems based on fuel cell technologies, due to the obstacles upon experimental studies, numerical modeling plays a central role to explore the performance of the system in a wide range of operating parameters [16,17]. Lunghi et al. [18] studied an MCFC-GT hybrid system and performed a system optimization by varying the fuel cell size and the fuel utilization coefficient. Moreover, an MCFC operated at ambient pressure and combined with an

* Corresponding author. Tel.: +61 413077896.
E-mail addresses: alireza.haghighat@mail.polimi.it (A. Haghighat Mamaghani), behzad.najafi@polimi.it (B. Najafi), a.shirazi@student.unsw.edu.au (A. Shirazi), fabio.rinaldi@polimi.it (F. Rinaldi).

Nomenclature

Acronyms

GA	genetic algorithm
LMTD	logarithmic mean temperature difference
MCFC	molten carbonate fuel cell
ORC	organic Rankine cycle
WGS	water gas shift

Symbols

A	area (m^2)
c_f	unit cost of fuel (€ MJ^{-1})
CRF	capital recovery factor
$\dot{C}_{env}$	social cost of air pollution (€ s^{-1})
$\dot{C}_{tot}$	total cost rate (€ s^{-1})
D	diameter (m)
E	open circuit voltage (V)
ex	exergy per unit mass (kJ kg^{-1})
$\dot{E}$	exergy flow rate (kW)
E_{act}	activation energy (kJ mol^{-1})
$\overline{e}$	standard chemical exergy (kJ $kmol^{-1}$)
f	Darcy friction factor
F	Faraday constant (96,485C mol^{-1})
G	mass flux (kg m^{-2} s^{-1})
ΔG	Gibbs free energy (J mol^{-1})
h	specific enthalpy on a mass basis (kJ kg^{-1})
$\overline{h}$	specific enthalpy on a molar basis (kJ $kmol^{-1}$)
ΔH	enthalpy (kJ $kmol^{-1}$)
I	current (A)
i	interest rate (%)
j	current density (A m^{-2})
k	thermal conductivity (W/m K)
K	equilibrium constant
L	length (m)
LHV	lower heating value (kJ kg^{-1})
$\dot{m}$	mass flow rate (kg s^{-1})
M	molar mass (kg $kmol^{-1}$)
N	operational hours in a year
n	system lifetime (year)
$\dot{n}$	molar flow rate (kmol s^{-1})
p	pressure (Pa or bar)
Pr	Prandtl number
Nu	Nusselt number
q″	specific heat power (W m^{-2})
$\dot{Q}$	heat transfer rate (kW)
R	resistance (Ω)
R_u	universal gas constant (J mol^{-1} K^{-1})
Re	Reynolds number
r	pressure ratio
s	specific entropy on a mass basis (kJ kg^{-1} K^{-1})
$\overline{s}$	specific entropy on a molar basis (kJ $kmol^{-1}$ K^{-1})
S/C	steam to carbon ratio
T	temperature (K)
TIT	turbine inlet temperature (K)
U	overall heat transfer coefficient (W/m^2 K)
U_f	fuel utilization factor
V	voltage (V)
$\dot{W}$	power (kW)
x	molar fraction
Z	capital cost in €
$\dot{Z}$	capital cost rate (€ s^{-1})

Greek symbols

α	convective heat transfer coefficient (W m^{-2} K^{-1})
η	efficiency
Φ	maintenance factor
Ψ	exergetic efficiency
μ	viscosity (Pa s)
ρ	density (kg/m^3)
ε	effectiveness

Subscripts

an	anode
B	burner
cat	cathode
C	compressor
CC	combustion chamber
Ch	chemical
cond	condenser
D	destruction
el	electrical
env	environmental
evap	evaporator
ex	exergetic
exp	expander
f	fuel
g	electric generator
gen	generated
HE-1	heat exchanger
ir	internal
M	mixer
motor	electrical motor
ne	nernst
o:	outside
Ph	physical
pp	pinch point
preh	preheater
R	reformer
red	reduced
RHE	recovery heat exchanger
T	gas turbine
tot	total
wf	working fluid

STIG cycle was investigated by Ubertini and Lungh [19] and efficiencies up to 69% were obtained. Another study conducted by Varbanov et al. [20] revealed that coupling a steam generation power system with an MCFC plant leads to about 24% improvement in the overall thermal efficiency of the system.

ORC cycle can be employed downstream of the gas turbine to extract the remaining waste heat from the exhaust gases and provide even higher overall power output [21,22]. Akkaya and Sahin [23] studied the energetic performance of a combined system consisting of an SOFC and an ORC running with R-113. The results showed that the efficiency of the SOFC-ORC system is 14–25% higher than the efficiency of a single SOFC because of the waste heat recovery through ORC. Moreover, Al-Sulaiman et al. [24] suggested a tri-generation plant based on coupling an SOFC to an

ORC can improve the efficiency by 22%. In a recent study [22], an SOFC-GT-ORC combined system was examined from thermodynamic standpoint and the results showed that an overall electrical efficiency of 67.4% can be obtained.

Exergetic analysis, based on the second law of thermodynamics, is a valuable method which enables the identification of the source and magnitude of exergy destruction in a given process [25]. Rashidi et al. [26] performed an exergetic investigation on an MCFC-GT system, and reported overall energetic and exergetic ef-ficiencies of 57.4% and 56.2% respectively. Shirazi et al. [27] con-ducted thermal-economic-environmental analyses and multi-objective optimization on an SOFC-GT. Moreover, Silveira et al.[28] implemented the energetic and exergetic analysis for an MCFC-based cogeneration system to produce electricity and cold water, achieving a global efficiency of 86%.

Numerous studies have been done on the economic analysis of power plants equipped with MCFCs. As a case in point, Verda and Nicolin [29] studied the thermo-economic optimization of an MCFC-GT hybrid system coupled with a pressure swing absorption system for the combined electricity and hydrogen production. The results suggested that the designs corresponding to the maximum and minimum electrical efficiencies, 0.62 and 0.46, lead to the maximum and minimum costs of electricity, 0.055 and 0.036 USD per kWh respectively. In order to boost the efficiency of a 250 kW SOFC system on board a ship, Ghirardo et al. [30] employed an organic Rankine bottoming cycle, resulting in a 35 kW extra elec-tricity generation and 5% enhancement in the overall efficiency. There are limited studies in which the environmental aspect of MCFC units is considered. Monaco and Di Matteo [31] performed a life cycle analysis of an MCFC unit in order to investigate the environmental impact associated with this system. Moreover, Sanchez et al. [32] propounded the MCFC unit as an active carbon sequestration device which not only produces electricity but also captures CO_2 at the same time.

In this study, a comprehensive modeling and optimization of MCFC-GT-ORC hybrid plant is conducted, taking into account the energetic, exergetic, economic and environmental aspects of the system (4E analysis). As such, a complete thermodynamic model of a hybrid MCFC-GT-ORC plant is firstly represented, enabling the evaluation of energetic and exergetic efficiencies of the plant. An economic model for the total cost rate of the plant, comprising the capital, operating and environmental costs is developed. In order to evaluate the environmental impacts, the social penalty cost associated with CO, NO_x, and CO_2 emissions of the plant is determined. By employing the GA (genetic algorithm) optimization method, the multi-objective optimization of the system is performed. TOPSIS (technique for order preference by similarity to an ideal solution) decision making method is applied to choose the final optimum design point of the system. Finally, in order to provide a better insight into the plant's behavior and to investigate the effect of variations in some of the economic parameters, a sensitivity analysis was performed on the Pareto front solutions with respect to the unit cost of fuel and the interest rate.

2. Plant description

The general schematic of the system is shown in Fig. 1. The system is mainly composed of an MCFC plant and an ORC (organic Rankine cycle) as the bottoming unit. Natural gas, considered to be pure methane, is used as the system fuel input which is converted into a hydrogen-rich mixture in the reformer. The mixture of water vapor and methane is preheated in the heat exchanger and is subsequently fed to the reformer where reforming reactions occur. The required heat for the endothermic reactions (except the WGS (water gas shift)) in the reformer is supplied by the catalytic burner which burns the anode outlet stream containing unreacted methane, hydrogen and carbon monoxide. The hydrogen-rich stream exchanges heat with the reformer inlet stream and cools down to reach the desired temperature, and then enters the anode side of the MCFC stack to participate in the electrochemical reaction. On the other side, the air stream entering the plant is pressurized by the air compressor and then is mixed with the high temperature outlet stream of the catalytic burner to provide the required amount of oxygen and carbon dioxide for electrochemical reaction in the cathode side of the MCFC.

Part of the cathodic outlet stream is directed to the combustion chamber where the residual carbon monoxide is burnt together with the appropriate amount of fuel. The resulting flue gas in burner has a high amount of energy which can be extracted through the turbine which not only does meet the compressor required power but also provides further electrical power. The waste heat in the flue gas leaving the MCFC-GT plant can be utilized by means of a bottoming cycle. The working fluid in the ORC subsystem is toluene which in the first step is vaporized in the evaporator, recovering the heat of the flue gas. The stream leaving the evaporator enters the ORC turbine where the required power of the ORC compressor and additional power are produced. Finally, the turbine outlet stream is cooled down in the water cooled condenser and is pumped back to the evaporator.

3. Energy analysis

The following assumptions were made to develop the thermodynamic model of the plant:

- Steady state operation is considered for all components.
- Air at the inlet of the compressor consists of 79% N_2 and 21% O_2.
- Constant and equal pressures in the fuel cell gas flow channels.
- Cathode and anode temperature are supposed to be the same at the outlets.
- Pressure at the anode and the cathode of the MCFC is considered to be constant and equal.
- There are no heat losses from the reformer, fuel cell stack, and the burner to the surroundings.
- Heat exchangers, mixers, pump, compressors and the turbines are adiabatic; hence, there is no heat transfer between these systems and the surrounding environment.
- Combustion chamber is non-adiabatic and 2% of the total generated heat is transferred to the environment.
- Electrolyte migration in the fuel cell stack is considered negligible.
- The working fluid in ORC cycle is pure Toluene.

For all components, energy and mass balances have been considered to perform the simulation and modeling.

3.1. Air compressor

The required power consumed by the air compressor to increase the pressure of inlet air to the desired pressure is supplied by the gas turbine. The isentropic efficiency of the compressor (η_C) is defined as follows:

$$\eta_C = \frac{h_{8,S} - h_7}{h_8 - h_7} \tag{1}$$

Applying the energy balance on the compressor, the compressor's required power can be expressed as:

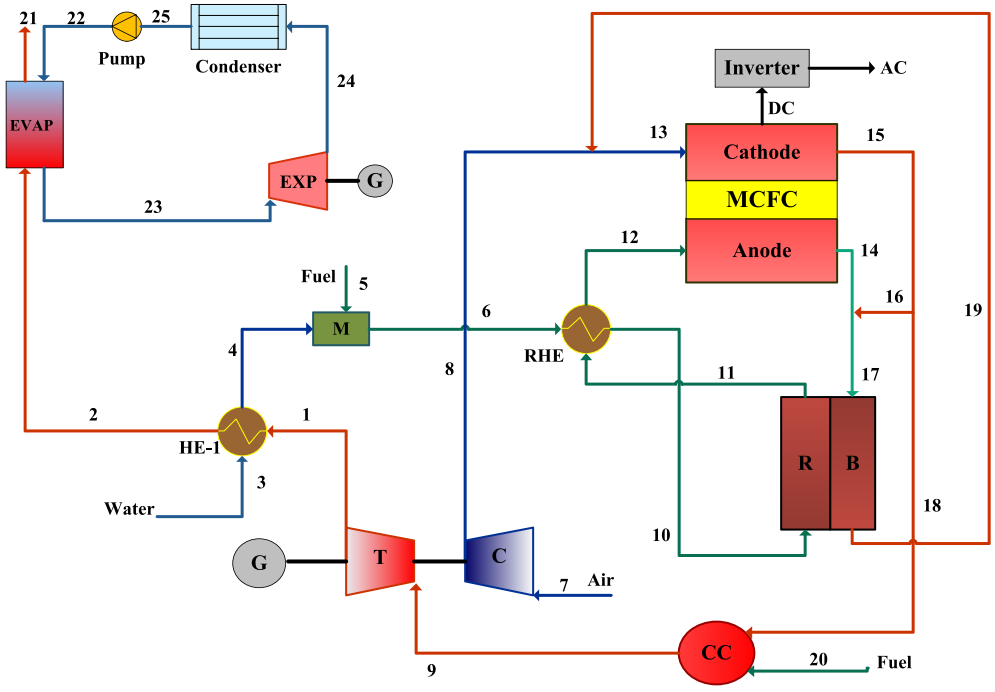

Fig. 1. Schematic diagram of the MCFC-GT-ORC power system.

$$\dot{W}_C = \dot{m}_8 h_8 - \dot{m}_7 h_7 \tag{2}$$

3.2. Gas turbine

Gas turbine provides the required power of the air compressor and also additional useful work which results in electrical power generation.

Considering the following definition for the isentropic efficiency of the turbine, the outlet temperature of the gas turbine can be calculated:

$$\eta_T = \frac{h_9 - h_1}{h_9 - h_{1,s}} \tag{3}$$

The mechanical work of gas turbine is determined as follows:

$$\dot{W}_T = \dot{m}_9 h_9 - \dot{m}_1 h_1 \tag{4}$$

3.3. Heat exchangers

The heat exchangers are modeled employing the ε-NTU method in which the effectiveness can be calculated using effective heat transfer coefficient and surface area.

The effectiveness of the heat exchanger is defined as:

$$\varepsilon = \frac{C_{cold}\left(T_{cold,out} - T_{cold,in}\right)}{C_{\min}\left(T_{hot,in} - T_{cold,in}\right)} \tag{5}$$

where C_{cold} is the heat capacity rate of the cold flow, and the C_{min} is the minimum between C_{cold} and the heat capacity rate of the hot flow (C_{hot}).

It is worth mentioning that since there is no heat loss from heat exchangers, the energy balance can be considered as:

$$\dot{m}_{hot,in} h_{hot,in} + \dot{m}_{cold,in} h_{cold,in} = \dot{m}_{hot,out} h_{hot,out} + \dot{m}_{cold,out} h_{cold,out} \tag{6}$$

3.4. Reformer

In order to provide the required fuel of anode side, which is hydrogen, the mixture of preheated steam and methane enters the reformer and the hydrogen-rich flow leaves this component. Reactions occurring in the reformer are mainly endothermic (except for the water gas shift reaction) and the required energy $\dot{Q}_B$ is supplied by the hot flue gas from the burner which can be obtained considering the energy balance around the catalytic burner.

Xu and Froment [33] proposed a general Langmuir–Hinshelwood type kinetic model for the steam reforming of methane using a Nickel based catalyst considering the water–gas shift reaction to occur in parallel with the steam reforming reactions. Consequently, the following reactions are considered to take place in the reactor:

$$CH_4 + H_2O \Leftrightarrow CO + 3H_2 \tag{7}$$

$$CH_4 + CO_2 \Leftrightarrow 2CO + 2H_2 \tag{8}$$

$$CO + H_2O \Leftrightarrow CO_2 + H_2 \tag{9}$$

The corresponding kinetics equations are as follows:

$$r_1 = \frac{k_1}{p_{H_2}^{2.5}} \frac{p_{CH_4} p_{H_2} - p_{H_2}^3 p_{CO}/K_1}{DEN^2} \tag{10}$$

$$r_2 = \frac{k_2}{p_{H_2}} \frac{p_{CO} p_{H_2O} - p_{H_2} p_{CO_2}/K_2}{DEN^2} \tag{11}$$

$$r_3 = \frac{k_3}{p_{H_2}^{3.5}} \frac{p_{CH_4} p_{H_2O}^2 - p_{H_2}^4 p_{CO_2}/K_3}{DEN^2} \tag{12}$$

where p_i is the partial pressure of the species "i" in the mixture and:

$$DEN = 1 + K_{CO}p_{CO} + K_{H_2}p_{H_2} + K_{CH_4}p_{CH_4} + \frac{K_{H_2O}p_{H_2O}}{p_{H_2}} \quad (13)$$

$$k_i = A(k_i)\exp\left[-E_{act,i}/(R_uT)\right], \quad \text{for } i = 1,\ldots,3 \quad (14)$$

$$K_i = A(K_i)\exp\left[-\Delta G_i^{\circ}/(R_uT)\right], \quad \text{for } i = 1,\ldots,3 \quad (15)$$

$$K_j = A(K_j)\exp\left[-\Delta H_j^{\circ}/(R_uT)\right], \quad \text{for } j = CH_4, H_2O, CO, H_2 \quad (16)$$

The kinetic parameters of the above reaction rates and the applied correlations for heat transfer inside the reformer can be found in Ref. [33].

3.5. MCFC stack

The basic concept of molten carbonate fuel cell is similar to the other kinds of fuel cell, which is the electricity generation via electrochemical reactions. In the anodic side, the hydrogen generated in the reformer reacts with carbonate ions (CO_3^{2-}) which have passed through the membrane and produce water, carbon dioxide and electrons. These produced electrons are transferred through an external circuit and generate electrical power and then enter the cathodic side of the stack where they react with oxygen from the air flow and carbon dioxide from recycle stream at the outlet of the cathode. Alongside the electrochemical reaction, water gas shift reaction, due to the presence of CO, occurs in the anodic side. The chemical reactions taking place inside the stack are shown below:

Anodic side:

$$2H_2 + 2CO_3^{2-} \rightarrow 2H_2O + 2CO_2 + 4e^-$$

$$CO + H_2O \leftrightarrow CO_2 + H_2 \text{ (water-gas shift reaction)}$$

Cathodic side:

$$O_2 + 2CO_2 + 4e^- \leftrightarrow 2CO_3^{2-}$$

The overall reaction:

$$½\ O_2 + H_2 \rightarrow H_2O$$

The molten carbonate fuel cell is made up of the anode, the cathode and the electrolyte, but for the subsequent analyses (mass, energy and exergy) of the stack we consider the MCFC as a single unit.

The equilibrium constant of the water gas shift reaction can be calculated using the following relation [34]:

$$K_{WGS} = e^{\frac{4276}{T} - 3.961} \quad (17)$$

where T is the temperature of the stack in kelvin. The equilibrium constant of shifting reaction can also be expressed in terms of partial pressures:

$$K_{WGS} = \frac{p_{CO_2}p_{H_2}}{p_{CO}p_{H_2O}} \quad (18)$$

Assuming that y and x are the molar flow rates of H_2 and CO participating in the electrochemical and water gas shift reactions respectively:

$$K_{WGS} = \frac{(\dot{n}_{CO_2,12} + x + y)(\dot{n}_{H_2,12} + x - y)}{(\dot{n}_{CO,12} - x)(\dot{n}_{H_2O,12} - x + y)} \quad (19)$$

$$y = U_f\left(\dot{n}_{H_2,12} + x\right) \quad (20)$$

$$U_f = \frac{\dot{n}_{H_2,12} - \dot{n}_{H_2,14}}{\dot{n}_{H_2,12}} \quad (21)$$

With the knowledge of the stack temperature, the equilibrium constant can be calculated from Eq. (17), and x and y are determined by solving Eqs. (19) and (21) simultaneously.

3.5.1. Current, current density, cell potential and resistances

The MCFC fuel cell current (I) can be calculated based on the molar flow rate of consumed hydrogen (y) during the electrochemical reaction in the fuel cell as follows:

$$I = 2Fy \quad (22)$$

where F is the Faraday constant.

The fuel cell operating voltage can be determined using the following equation:

$$V_{cell} = E - \eta_{ne} - IR_{tot} \quad (23)$$

where E is the maximum theoretically achievable reversible potential, η_{ne} is the Nernst loss, I is the current, and R_{tot} is the sum of resistances in the an (anode), ca (cathode) and the internal resistance [35]. The term E can be determined as follows:

$$E = \frac{-\Delta G}{2F} \quad (24)$$

where ΔG is the change in molar Gibbs free energy of formation at standard pressure, The Gibbs free energy change can be expressed as function of temperature:

$$\Delta G = -242000 + 45.8T \quad (25)$$

where T is the stack temperature in kelvin.

$$\eta_{ne} = \frac{R_uT}{2F} \times \ln\frac{p_{CO_2,cat}p_{H_2,an}p_{O_2,cat}^{0.5}}{p_{H_2O,an}p_{CO_2,an}} \quad (26)$$

$$y = U_f\left(\dot{n}_{H_2,12} + x\right) \quad (27)$$

where p is the species average partial pressure in cell, and 'an' and 'cat' denote anodic and cathodic sides, respectively.

Due to voltage losses corresponding to the anodic, cathodic and internal resistances, the actual voltage of the cell is less than the ideal one. The total resistance in the stack (R_{tot}) can be defined as follows:

$$R_{tot} = R_{an} + R_{cat} + R_{ir} \quad (28)$$

where R_{an} and R_{cat} are the anode and cathode resistances due to the polarization in the respective electrodes, and R_{ir} is the internal cell resistance which is referring to the resistance to the electron transport within the bipolar plates and the ion transport through the electrolyte. The following equations can be used to calculate the foregoing resistances [34]:

$$R_{an} = C_a e^{\frac{\Delta H_a}{R_u T}} P_{H_2,an}^{-0.5} A^{-1} \tag{29}$$

$$R_{cat} = C_1 e^{\frac{\Delta H_{C1}}{R_u T}} P_{O_2,cat}^{-0.75} P_{CO_2,cat}^{0.5} + C_2 e^{\frac{\Delta H_{C2}}{R_u T}} C_{CO_2,cat}^{-1} A^{-1} \tag{30}$$

$$R_{ir} = C_{ir} e^{\frac{\Delta H_{ir}}{R_u T}} A^{-1} \tag{31}$$

where C_i coefficients are the parameters related to electrodes and electrolytes, P and ΔH are the pressure (atm) and the enthalpy (J mol^{-1}) respectively. From theses equations, it can be observed that resistances in anodic and cathodic sides mainly depend on temperature and partial pressures of the gases, H_2 at anode, CO_2 and O_2 at cathode, and some parameters related to electrodes and electrolyte.

The electrical power generated by the stack $\dot{W}_{MCFC}$(kW) is expressed as follows:

$$\dot{W}_{MCFC} = V_{cell} j A \tag{32}$$

The thermal energy generated within the MCFC stack by electrochemical and water gas shift reactions can be achieved from:

$$\dot{Q}_{gen,MCFC} = I \Delta V_{loss} \times 10^{-3} + T \Delta S \tag{33}$$

where

$$\Delta S = y \left[\left(\bar{s}_{H_2O}^0 - \bar{s}_{H_2}^0 - \frac{1}{2} \bar{s}_{O_2}^0 \right) - R_u \ln \frac{p_{H_2O}}{p_{H_2} p_{O_2}^{0.5}} \right] \tag{34}$$

where $\bar{s}^0$ is the entropy at standard temperature and pressure.

$$\dot{Q}_{WGS} = x \left(\bar{h}_{CO_2} + \bar{h}_{H_2} - \bar{h}_{CO} - \bar{h}_{H_2O} \right) \tag{35}$$

In order to determine the net thermal energy generated in the stack which heats up the outlets flows from anodic and cathodic sides both $\dot{Q}_{gen,MCFC}$ and $\dot{Q}_{WGS}$ should be taken into account:

$$\dot{Q} = \dot{Q}_{gen,MCFC} - \dot{Q}_{WGS} \tag{36}$$

On the other hand, this value, net thermal energy, can be determined from the rate of the enthalpy changes of reactants and products at the cathodic and anodic sides as follows:

$$\dot{Q}' = \dot{m}_{12} h_{12} + \dot{m}_{13} h_{13} - \dot{m}_{14} h_{14} - \dot{m}_{15} h_{15} \tag{37}$$

Writing energy balance equation over the MCFC stack, the temperature of the stack can be determined through an iterative procedure. The iteration will stop when the desired error is reached:

$$error = abs \left(\frac{\dot{Q}' - \dot{Q}}{\dot{Q}} \right) < 0.03 \tag{38}$$

In order to solve the total thermal balance of the plant, guess values are first assumed for the temperature of the stack and the molar flow rates of anodic and cathodic outlets. Afterwards, a loop is considered around the reformer, burner and the RHE to find the inlet temperatures to the stack as well as the turbine inlet mass flow rate. Considering the created calculation loops, the iterative procedure is continued until the convergence is reached and the difference between the obtained values and assumed ones is less than the specified tolerance.

3.6. ORC unit

Recovering the low grade heat from the flue gases leaving the plant, ORC can significantly boost the overall electrical efficiency of the system. Due to the low temperature and pressure of the exiting flue gas, utilizing steam cycles would be pointless and not efficient [36]. Selection of suitable working fluid, mainly according to the waste heat temperature, is a key step in implementation of an ORC system. Numerous thorough studies can be found in literature proposing different strategies and criteria for the working fluid selection [37,38]. Toluene has been chosen as the working fluid in this study due to its viability for medium and large scale power generations [37]. The main components in ORC system are expander, condenser, and evaporator and pump which have been extensively investigated since their performance directly influences the overall efficiency and power output of the bottoming cycle.

3.6.1. Evaporator

Evaporator is the main component in the ORC cycle since it dictates the amount of heat that can be transferred from the hot waste flue gases to the working fluid for power generation within the ORC expander. In the present study, preheating and evaporation are conducted in the evaporator as superheating toluene at the expander inlet is not recommended due to the significant drop in the efficiency of the bottoming cycle [37]. A finned-tube heat exchanger has been used in this study to model the evaporator of the ORC unit. The design details and correlations of this heat exchanger were taken from Ref. [39]. The geometric parameters for the evaporator are presented in Table 1. The LMTD (logarithmic mean temperature difference) Method is employed to determine the heat transfer area of both preheater and evaporator zones. Accordingly, for the evaporator:

$$\dot{Q}_{preh} = U_{preh} A_{o,preh} LMTD_{preh} \tag{39}$$

$$\dot{Q}_{evap} = U_{evap} A_{o,evap} LMTD_{evap} \tag{40}$$

The global coefficients are calculated based on outside area as:

$$U_{preh} = \frac{1}{\frac{1}{\alpha_{gas} \eta_o} + \frac{\ln(D_o/D_i)}{2\pi L_{tot,preh} k_{tube}} + \frac{A_{o,preh}}{\alpha_{preh} A_{i,preh}}} \tag{41}$$

$$U_{evap} = \frac{1}{\frac{1}{\alpha_{gas} \eta_o} + \frac{\ln(D_o/D_i)}{2\pi L_{tot,evap} k_{tube}} + \frac{A_{o,evap}}{\alpha_{evap} A_{i,evap}}} \tag{42}$$

Since both heat exchanger area and overall heat transfer coefficient are unknown, an iterative procedure has been employed for each zone to find the heat transfer area and the overall heat transfer coefficient.

Table 1
Fixed geometric parameters of the ORC evaporator.

Parameter	Description	Value
D_o	Outer diameter tube	0.027 m
D_i	Inner diameter tube	0.020 m
L	Tube length	8 m
k	Thermal conductivity	17 W/mK
CP	Column pitch	0.054 m
RP	Row pitch	0.04677 m
H	Fin height	0.027 m
Y	Fin thickness	0.004 m
S	Fin spacing	0.016 m
z	Fin density	50 fin/m

For the flue gas side (outside of tubes), the convective heat transfer coefficient can be calculated with the following correlation:

$$Nu_{gas} = \frac{D_o \alpha_{gas}}{k_{gas}} = 0.1378 \left(\frac{D_o G_{\max}}{\mu_{gas}}\right)^{0.718} \mathrm{Pr}_{gas}^{1/3} \left(\frac{S}{H}\right)^{0.296} \quad (43)$$

For the single-phase working fluid flowing within the tube, in the preheater, the Gnielinski correlation has been used [40]:

$$Nu_{preh} = \frac{\frac{f}{8}\left(\left(\mathrm{Re}_{wf} - 1000\right)\mathrm{Pr}_{wf}\right)}{1 + 12.7\sqrt{\frac{f}{8}}\cdot\left(\mathrm{Pr}_{wf}^{2/3} - 1\right)} \cdot \left[1 + \left(\frac{D_i}{L}\right)^{2/3}\right] \quad (44)$$

In addition, considering the working fluid in the two-phase zone, the experimental results by Huang et al. [41] suggested that the Liu and Winterton correlation can accurately predict the convective heat transfer coefficient.

$$\alpha_{evap,j} = \sqrt{\left(E\alpha_{f0}\right)^2 + \left(F\alpha_{nb}\right)^2} \quad (45)$$

where correction factor for the film boiling, E, can be defined as:

$$E = \left[1 + x_j \mathrm{Pr}_{liq}\left(\frac{\rho_{liq}}{\rho_{vap}} - 1\right)\right]^{0.35} \quad (46)$$

The convective heat transfer coefficient for film boiling, α_{f0}, computation is based on the Dittus–Boelter correlation:

$$Nu_{liq} = 0.023\mathrm{Re}_{liq}^{0.8}\mathrm{Pr}_{liq}^{0.4} \quad (47)$$

The correction factor for the nucleate boiling F is:

$$F = \frac{1}{1 + 0.55E^{0.1}\mathrm{Re}_{f0}^{0.16}} \quad (48)$$

The Reynolds number corresponding to the saturated liquid state is expressed by:

$$\mathrm{Re}_{f0} = \frac{G(1 - x_j)D_i}{\mu_{liq}} \quad (49)$$

The convective heat transfer coefficient for the nucleate boiling α_{nb} is calculated according to the pool boiling correlation of Copper as in Bertsh et al. [42], that results to be suitable for toluene [43]:

$$\alpha_{nb} = 55 \cdot p_{red}^{0.12}(-0.4343 \ln p_{red})^{-0.55} M^{-0.5} \left(q''\right)^{0.67} \quad (50)$$

where p_{red} is the reduced pressure (kPa), M is the molar mass (kg kmol^{-1}) and q″ is the specific heat power (W m^{-2}).

3.6.2. Expander

In the expander, a non-isentropic expansion process can be described by the isentropic efficiency, which can be expressed as

$$\eta_{\exp} = \frac{h_{23} - h_{24}}{h_{23} - h_{24,s}} \quad (51)$$

The work output of the expander can be expressed as:

$$\dot{W}_{\exp} = \dot{m}_{wf} \cdot (h_{23} - h_{24}) \quad (52)$$

where $\dot{m}_{wf}$ is the working fluid mass flow rate.

3.6.3. Pump

The ORC pump power consumption ($\dot{W}_{pump}$) is determined based on the following formulae:

$$\dot{W}_{pump} = \frac{\dot{m}_{wf} \times (p_{22} - p_{25})}{\rho_{wf} \times \eta_{pump}} \quad (53)$$

where η_{pump} is the pump isentropic efficiency.

4. Exergetic analysis

Exergetic analysis is a branch of applied thermodynamics which is based on the second law of thermodynamics. This type of analysis focuses not only on the quantity of energy, but also on its quality [44].

By employing the first and second laws of thermodynamics, the steady state exergy balance equation can be written as:

$$\frac{dE_{CV}}{dt} = \sum_j \dot{E}_j^Q - \dot{E}^W + \sum_i \dot{E}_i - \sum_e \dot{E}_e - \dot{E}_D = 0 \quad (54)$$

where the terms $\dot{E}_j^Q$, $\dot{E}^W$, and $\dot{E}_D$ are the exergy transfer associated with heat transfer, the exergy transfer accompanying net useful work, and the exergy destruction, respectively, $\dot{E}_i$ and $\dot{E}_e$ are the exergy transfer rate at inlets and outlets.

Assuming negligible values of change in potential and kinetic exergy, the exergy flow rate of the system can be expressed as:

$$\dot{E} = \dot{E}_{Ph} + \dot{E}_{Ch} \quad (55)$$

$$\dot{E}_{Ph} = \dot{m}[(h - h_0) - T_0(s - s_0)] \quad (56)$$

$$\dot{E}_{Ch} = \dot{n}\left[\sum_k x_k \bar{e}_k + \bar{R}T_0 \sum_k x_k \ln x_k\right] \quad (57)$$

By taking into account the exergy balance equation for each system component, the exergy destruction rate of each component can be determined as presented in the Table 2.

5. Economic analysis

Besides being energy efficient, a power generation system should also be economically viable and cost efficient. The system total cost in this paper is one of objective functions aimed to be minimized. The total cost includes capital and maintenance expenses, the system operating cost (fuel cost), as well as the environment related costs. The investment cost functions are listed in

Table 2
Exergy destruction rate for each component of the system.

System component	Exergy destruction rate
Compressor	$\dot{E}_{D,C} = \dot{E}_7 - \dot{E}_8 + \dot{W}_C$
Combustion chamber	$\dot{E}_{D,CC} = \dot{E}_{20} + \dot{E}_{18} - \dot{E}_9$
Turbine	$\dot{E}_{D,T} = \dot{E}_9 - \dot{E}_1 - \dot{W}_T$
Reformer and Burner	$\dot{E}_{D,B-R} = \dot{E}_{17} + \dot{E}_{10} - \dot{E}_{18} - \dot{E}_{11}$
Heat exchanger	$\dot{E}_{D,HE-1} = \dot{E}_1 + \dot{E}_3 - \dot{E}_2 - \dot{E}_4$
Recovery heat exchanger	$\dot{E}_{D,RHE} = \dot{E}_6 + \dot{E}_{11} - \dot{E}_{10} - \dot{E}_{12}$
MCFC stack	$\dot{E}_{D,MCFC} = \dot{E}_{12} + \dot{E}_{13} - \dot{E}_{14} - \dot{E}_{15} - \dot{W}_{MCFC}$
ORC pump	$\dot{E}_{D,P} = \dot{E}_{25} - \dot{E}_{22} + \dot{W}_P$
ORC evaporator	$\dot{E}_{D,EVA} = \dot{E}_2 + \dot{E}_{22} - \dot{E}_{21} - \dot{E}_{23}$
ORC expander	$\dot{E}_{D,EXP} = \dot{E}_{23} - \dot{E}_{24} - \dot{W}_{EXP}$
ORC condenser	$\dot{E}_{D,CON} = \dot{E}_{24} + \dot{E}_{water,in} - \dot{E}_{25} - \dot{E}_{water,out}$

Table 3 for major components in terms of their design parameters. The target cost for MCFC has been estimated to be 2600 €/kW in the previous studies, and the same cost was considered in the present study [8]. In order to evaluate the capital cost per unit of time ($\dot{Z}_k$) the following correlation has been employed:

$$\dot{Z}_k = \frac{Z_k \times CRF \times \phi}{N \times 3600} \tag{58}$$

where N, ϕ, and CRF (capital recovery factor) are the annual operational hours of the system, maintenance factor, and the Capital Recovery Factor, respectively. CRF can be determined with the following relation:

$$CRF = \frac{i(1+i)^n}{(1+i)^n - 1} \tag{59}$$

where i is the interest rate and n is the equipment lifetime. In addition, the operational cost of the system can be estimated by:

$$\dot{C}_f = \frac{c_f LHV \dot{m}_f}{1000} \tag{60}$$

wherec_f is the unit cost of the fuel, LHV is the lower heating value, and $\dot{m}_f$ is the total mass flow rate of fuel enters the plant.

6. Environmental analysis

The environmental issues are one of the major concerns which should be considered while analyzing a power production system. As a result, the environmental social cost ($\dot{C}_{env}$) has been considered in the total cost rate of the plant through the optimization of the MCFC-GT-ORC system. It is worth noting that no emission has been considered from the fuel cell stack; therefore, the catalytic burner and the combustion chamber are the only sources of environmental emissions. The environmental social cost of the plant can be calculated as follows:

$$\dot{C}_{env} = c_{CO}\dot{m}_{CO} + c_{CO_2}\dot{m}_{CO_2} + c_{NO_x}\dot{m}_{NO_x} \tag{61}$$

Table 3
The capital cost function of various components in the MCFC-GT-ORC hybrid plant [8,27,and36].

System component	Capital cost function
Compressor	$Z_C = \frac{39.5\times\dot{m}_a}{0.9-\eta_C}\left(\frac{P_{dc}}{P_{suc}}\right)\ln\left(\frac{P_{dc}}{P_{suc}}\right)$
Combustion chamber	$Z_{CC} = \left(\frac{46.08\times\dot{m}_{in}}{0.995-\frac{P_{out}}{P_{in}}}\right)[1+\exp(0.018T_{out}-26.4)]$
Turbine	$Z_T = \dot{W}_T[1318.5 - 98.328\ln(\dot{W}_T)]$
Reformer	$Z_R = 2860A_R^{0.69} + 28940V_R$
Heat exchanger	$Z_{HE} = 130\left(\frac{A_{HE}}{0.093}\right)^{0.78}$
Auxiliary device	$Z_{MCFC,aux} = 0.1(Z_{MCFC})$
MCFC stack	$Z_{MCFC} = 2600\dot{W}_{MCFC}$
Burner	$Z_B = \left(\frac{46.08\times\dot{m}_{in}}{0.995-\frac{P_{out}}{P_{in}}}\right)[1+\exp(0.018T_{out}-26.4)]$
ORC pump	$Z_P = 705.48\left(0.001\dot{W}_P^{0.71}\right)\left(1+\frac{0.2}{1-\eta_{S,P}}\right)$
ORC evaporator	$Z_{EVA} = \left(8500 + 406A_{eva+preh}^{0.85}\right)$
ORC expander	$Z_{EXP} = 1.5\left(225 + 170\dot{V}_{IN,\exp}\right)$
ORC condenser	$Z_{CON} = \left(8500 + 406A_{cond+precond}^{0.85}\right)$

where $\dot{m}_{CO}$, $\dot{m}_{NO_x}$, and $\dot{m}_{CO_2}$ are the exhaust mass flow rates of carbon monoxide, nitrogen monoxide, and carbon dioxide, and c_{NO_x},c_{CO} andc_{CO_2} are the unit damage costs of carbon monoxide, nitrogen monoxide, and carbon dioxide emissions, respectively. The amount of CO and NO_x produced in the burner in grams per kilogram of fuel can be estimated through the following equations:

$$m_{CO} = \frac{0.179\times10^9\times\exp\left(\frac{7800}{T_{pz}}\right)}{p^2\tau\left(\frac{\Delta p}{p}\right)^{0.5}} \tag{62}$$

$$m_{NO_x} = \frac{0.15\times10^{16}\times\tau^{0.5}\exp\left(\frac{-71100}{T_{pz}}\right)}{p^{0.05}\left(\frac{\Delta p}{p}\right)^{0.5}} \tag{63}$$

In these equations p is inlet pressure of combustion chamber, T_{pz} primary zone combustion temperature, τ residence time in the combustion zone, and $\frac{\Delta p}{p}$ the non-dimensional pressure drop in the combustion chamber [45,46].

7. Optimization

7.1. Objective functions and design parameters

In the present work, exergetic efficiency and the total cost rate of the system are considered as objective functions. A multi objective optimization is conducted aiming at maximizing the exergetic efficiency while the total cost rate of the system is minimized. The cost of the environmental damage is assumed to be added directly to the expenditures that must be paid. Therefore, the second objective function includes the rate of investment and maintenance costs ($\dot{Z}_K$), operational cost ($\dot{C}_f$), and the rate of penalty cost due to emissions ($\dot{C}_{env}$). The mathematical formulation of the objective functions can be written as follows:

$$Objective\ I = \Psi_{tot} = \frac{\dot{E}_{out}}{\dot{E}_{in}} = \frac{\dot{E}_{in} - \dot{E}_{D,tot}}{\dot{E}_{in}} = \frac{\dot{W}_{el,net}}{(\dot{m}_{20}+\dot{m}_5)\cdot ex_{CH_4}} \tag{64}$$

$$\dot{W}_{el,net} = \dot{W}_{MCFC}\eta_{DC/AC-inverter} + \left(\dot{W}_T - \dot{W}_C\right)\eta_g + \dot{W}_{\exp}\eta_g - \frac{\dot{W}_{pump}}{\eta_{motor}} \tag{65}$$

$$Objective\ II = \dot{C}_{tot} = \sum_k \dot{Z}_k + \dot{C}_f + \dot{C}_{env} \tag{66}$$

Moreover, the following design parameters are selected for the system optimization: S/C (steam to carbon ratio), r_C (air compressor pressure ratio), U_f (fuel utilization factor), η_T (gas turbine isentropic efficiency), TIT (turbine inlet temperature), T_{evap} (evaporation temperature), $\Delta T_{pp\text{-}evap}$ (evaporator pinch point temperature), T_{cond} (condensation temperature), and T_{cond} (condenser pinch point temperature). Table 4 represents the mentioned design parameters, their range of variation, and the constraints for system optimization.

7.2. Multi-objective optimization

Multi-objective optimization is an approach to find solutions to problems with conflicting objectives. Obviously, there is no single

Table 4
List of constraints for system optimization and the range of variation of design pa-rameters [10,29,36,and50].

Constraint	Reason
$2 < r_C < 16$	Typical technology and commercial availability
$0.6<\eta_T < 0.9$	Typical technology and commercial availability
$0.5 < U_f < 0.9$	Minimum and maximum values of fuel utilization factor
$2.5 < S/C < 5.5$	Minimum and maximum values of steam to carbon ratio
TIT<1250 K	The material limit of available technology
T_{MCFC}<1020 K	The material limit of available technology
$T_{21} > 350$ K	To avoid formation of carbonic acid (H_2CO_3) in exhaust gases
443K < T_{eva}<478 K	Typical data for ORC systems with Toluene as the working fluid
297K < T_{con}<323 K	Typical data for ORC systems with Toluene as the working fluid
3 K<$\Delta T_{pp\text{-}con}$<16 K	Minimum and maximum values of pinch point temperature in Condenser
4 K<$\Delta T_{pp\text{-}eva}$<25 K	Minimum and maximum values of pinch point temperature in Evaporator
$T_{23} < 671.9$ K	Maximum temperature beyond which degradation of the working fluid is expected to take place

solution which can comply with the conflicting objectives at the same time; therefore, the solution obtained for multi-objective optimization problems is a set of non-dominated solutions, called the Pareto Solution [47]. The Pareto set is the set of solutions with minimum conflict between objectives. The multi-objective optimization problem can be defined as:

$$Find\ \mathbf{x} = (\mathbf{x}_i)\ \ \forall i = 1, 2, \ldots, N_{par} \tag{67}$$

$$\text{Minimize or Maximize } f_i(\mathbf{x})\ \ \forall i = 1, 2, \ldots, N_{obj} \tag{68}$$

$$g_j(\mathbf{x}) = 0\ \forall j = 1, 2, \ldots, m \tag{69}$$

$$h_k(\mathbf{x}) \leq 0\ \ \forall k = 1, 2, \ldots, n \tag{70}$$

where $\mathbf{x}$, N_{par}, $f_i(\mathbf{x})$, N_{obj}, $g_j(\mathbf{x})$ and h_k $(\mathbf{x})$ are decision variables vectors, number of decision variables, objectives, number of objectives, equality and inequality constraints respectively [48].

7.3. Genetic algorithms

The GA (genetic algorithm) method is a heuristic technique utilized to find exact or approximate solutions to optimization problems. GA optimization procedure has been inspired by evolutionary theory of Charles Darwin "survival of the fittest" and natural genetics. Accordingly, the first step in GA is to provide a solution to the problem by a string of genes, known as a chromosome. In the next step, an initial population of legal chromosome is required to start the procedure.

The key advantage of using GA is the capability of this method to search in parallel, employing a population of points, which helps it to avoid being trapped in a local optimal solution. By taking advantage of genetic operators like crossover, mutation and selection, solutions become fitter and fitter as search starts, and finally it converges to a single solution. Mutation options determine how the GA makes small random changes in the individuals in the population to generate mutation children. Moreover, choice of parents for the next generation is done in the selection stage. Crossover options specify how the GA combines two individuals to form a crossover child for the next generation. The genetic process will stop if there is no change in the optimal values for a specified number of generations [49]. The flowchart in Fig. 2 represents various stages of GA optimization process. In the present study,

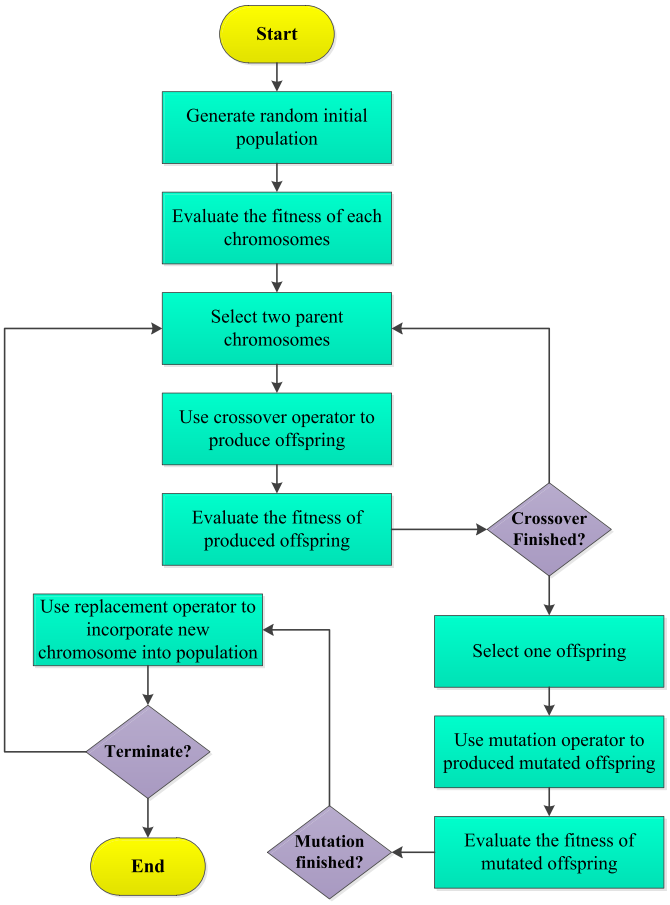

Fig. 2. Flowchart of genetic algorithm technique for plant optimization.

multi objective genetic algorithm implemented in MATLAB optimization toolbox has been employed. The genetic algorithm optimization was applied for 100 generations, using a search population size of 120 individuals, crossover probability 0.8, and gene mutation probability 0.01.

8. Performance indexes

In this section, the key indicators of the performance of the MCFC-GT-ORC plant are defined before further discussion on the obtained results. The total exergetic efficiency ($\eta_{ex,tot}$), MCFC system exergetic efficiency ($\eta_{ex,MCFC}$), and ORC cycle exergetic efficiency ($\eta_{ex,ORC}$) have been employed to investigate the performance of the proposed MCFC-GT-ORC system.

The total exergetic efficiency is defined as the net electrical power output divided by the total chemical exergy input to the system. Similarly, the MCFC system exergetic efficiency is defined as the ratio of power generated in the stack and the exergy input to the stack.

$$\eta_{ex,tot} = \frac{\dot{W}_{el,net}}{(\dot{m}_{20} + \dot{m}_5) \cdot ex_{CH_4}} \tag{71}$$

$$\eta_{ex,MCFC} = \frac{\dot{W}_{MCFC}}{\dot{E}_{12} + \dot{E}_{13}} \tag{72}$$

The ORC cycle exergetic efficiency is defined as the net electrical output of the bottoming cycle to the exergy input from the hot flue gases.

Table 5
Input parameters used for simulation of the MCFC-GT-ORC system [21,22,and24].

Parameter	Value
Ambient temperature	20 °C
Ambient pressure	1 bar
Air compressor isentropic efficiency	82%
Electrical generator efficiency	95%
Electrical motor efficiency	95%
DC-AC inverter efficiency	95%
ORC cycle pump isentropic efficiency	80%
ORC cycle turbine isentropic efficiency	80%
Fuel composition	CH_4 (100%)
Fuel LHV	50,009 (kJ kg^{-1})
Pressure loss	
Fuel cell stack	4%
Combustion chamber	5%
Recovery heat exchanger	3%

$$\eta_{ex,ORC} = \frac{\dot{W}_{\exp}\eta_g - \frac{\dot{W}_{pump}}{\eta_{motor}}}{\dot{E}_2 - \dot{E}_{21}} \quad (73)$$

9. Case study

The target city for the MCFC-GT-ORC hybrid system installa-tion has been chosen to be Milan, Italy. The ambient pressure and temperature which are considered in the optimization procedure are 1 bar and 20 °C respectively. Table 5 summarizes the main input parameters used in the modeling and simulation process. The total power output of the hybrid system (combi-nation of MCFC, gas turbine, and ORC cycle electrical outputs) is estimated to be 150 kW. In order to determine the CRF (Eq. (59)), the annual interest rate (i), approximate lifetime of the system (n), and the maintenance factor (F) are considered as 1.2%, 8 years (in case of MCFC stack we consider two 4 years periods by changing the stack after 4 years due to considerable voltage drop), and 1.08, respectively. The annual operational hours of the hybridsystem(N)is8000h.Theunitcostoffuel(c_f)is considered to be 0.0092 € MJ^{-1}. In addition, due to environmental concerns for pollutant emissions 0.01564 € $kg^{-1}CO$, 5.14 € $kg^{-1}NO_x$, and 0.0168 € $kg^{-1}CO_2$ as penalty are used for carbon monoxide (c_{CO}), nitrogen monoxide (c_{NOx}), and carbon dioxide (c_{CO}), respectively [27].

10. Results and discussion

10.1. Model validation

Fig. 3 demonstrates the voltage–current density curve of the MCFC stack at the considered operating pressure. To validate the MCFC stack behavior, a comparison has been made on the polarization curve generated by the present model and the one reported by Ref. [34]. Operating temperature and pressure are considered to be the same as the ones considered in the mentioned reference which are 950 K and 4 atm respectively. It should be noted that, in the present study, the range of the current density, in which the modeled fuel cell operates, is between 1500 and 3500 A/m^2. Accordingly, as can be seen in Fig. 3, the results of the present model are in close agreement with the results proposed by Baranak et al. [34], the fact which shows that our model is accurate enough to estimate the performance of MCFC stack in a sufficiently accurate way.

10.2. Optimization results

10.2.1. Pareto front

Fig. 4 demonstrates the Pareto frontier achieved from the multi-objective optimization of the MCFC-GT-ORC hybrid system using genetic algorithm. The conflicting relation between the two objective functions can be observed clearly from the represented figure. As shown in this figure, starting from the exergetic efficiency of 49.44%–52.25% only a slight increment in the total cost rate of the system would experience. However, after this point (i.e. exer-getic efficiency of 52.25%), by further increase in the exergetic ef-ficiency a steep rise in the total cost rate from 0.0098 € s^{-1} to 0.01106 € s^{-1} could be noticed. According to Fig. 4, the Pareto front curve represents two ultimate points (points A and B) where the optimization can be considered as a single objective function optimization. The highest exergetic efficiency is at design point (A)

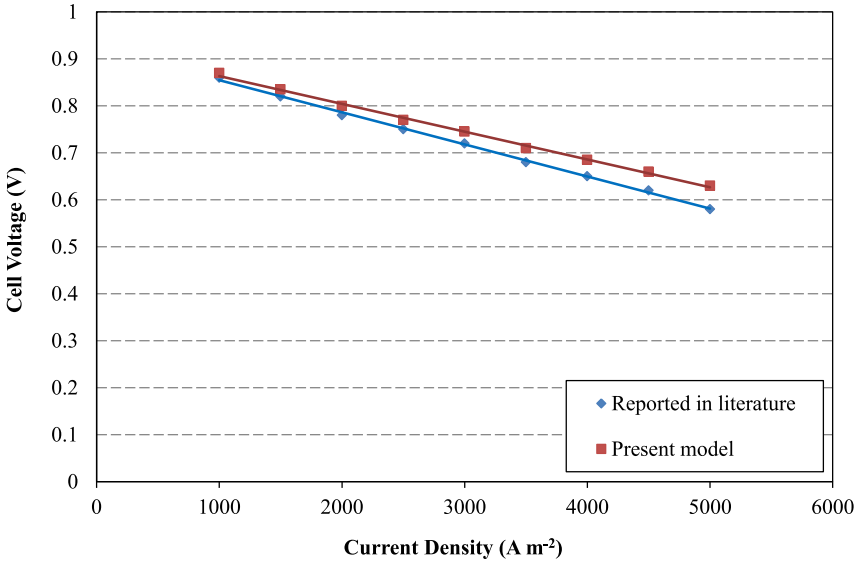

Fig. 3. Comparison between the current density-cell voltage curve generated by the results of the present model and the data from a previous study [34].

(56.06%), while the total cost rate has its highest value at this point (0.01106 € s^{-1}). On the other hand, the lowest exergetic efficiency, 49.44%, at design point B leads to the minimum total cost rate of the plant (0.00971 € s^{-1}). Point A represents the situation where the thermodynamic objective (exergetic efficiency) is most weighted, while point B has been mostly weighted in favor of economic objective (total cost rate of the system).

10.2.2. Selection of the final optimum design point

In order to select the most desirable optimum point amongst the Pareto front solutions, different techniques can be applied. For this purpose, in the current research after Euclidian non-dimensionalization of all objectives, TOPSIS (Technique for Order Preference by Similarity to an Ideal Solution) method has been used to specify the final optimum design point. In TOPSIS method, an ideal solution is an imaginary point where each objective has its optimum value while for the non-ideal solution each objective has its worst value. The two ideal and non-ideal solutions are shown on Fig. 5. The best optimal point will have the farthest distance from the non-ideal point and the shortest distance from the ideal point [50]. Following this method, the red highlighted point in Fig. 5 has been selected as the final optimum solution, corresponding to an exergetic efficiency of 54.95% and the total cost rate of 0.01023 € s^{-1}. The numerical values of optimum design parameters at point A, B, and the final optimum

Table 6
The optimum values of system design parameters from three optimization standpoints.

Design parameters	Point A as an extreme in favor of exergetic efficiency	Point B as an extreme in favor of total cost rate	Multi objective optimization (trade-off approach)
TIT (K)	1014	1009	1011.5
r_C	6.05	5.68	5.9
η_T (%)	87.4	86	89
U_f	0.61	0.602	0.65
S/C	4.31	4	5.25
T_{eva} (K)	466.65	468	466
$\Delta T_{pp\text{-}eva}$ (K)	9	10.4	9.7
T_{con} (K)	305	307.5	305.3
$\Delta T_{pp\text{-}con}$ (K)	6.5	6.9	6.65

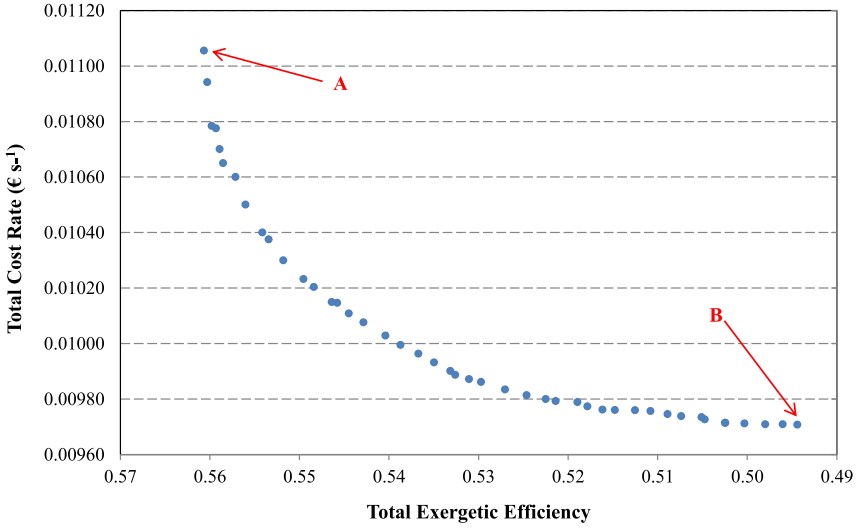

Fig. 4. Pareto front from multi-objective optimization of MCFC-GT-ORC plant.

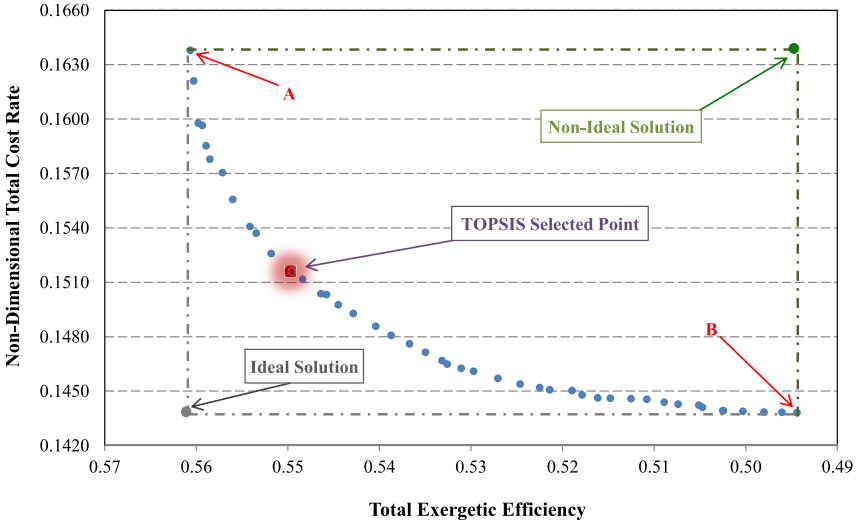

Fig. 5. Non-dimensional Pareto front for optimum point selection using TOPSIS decision-making method.

Table 7
Capital costs of major system components (in Euros).

Component	Point A as an extreme in favor of exergetic efficiency	Point B as an extreme in favor of total cost rate	Multi objective optimization (trade-off approach)
Compressor	5359	4822	5095
Turbine	75,780	74,730	80,685
Reformer	13,920	13,250	14,430
MCFC	594,442	485,515	529,852
Heat exchangers	5230	5009	5694
Expander	2220	1995	2100
Condenser	2374	2122	2268
Evaporator	10,881	9809	10,350

Table 9
Environmental performance of the plant from three optimization standpoints.

Parameter	Point A as an extreme in favor of exergetic efficiency	Point B as an extreme in favor of total cost rate	Multi objective optimization (trade-off approach)
NO emission (kg year^{-1})	13.8	13.5	13.7
CO emission (kg year^{-1})	345	408	323
CO_2 emission (kg year^{-1})	401,800	412,981	403,764
Social cost of air pollution (€ year^{-1})	6825	7015	6858
Share of the environmental cost in total cost rate (%)	2.14	2.5	2.33

point are listed in Table 6. As stated before, one of the main purposes of the present study is to evaluate the economic viability of the proposed system and also to underline the sig-nificance of using multi-objective optimization in finding the best trade-off between the economic indexes and thermody-namic performance. Table 7 presents the capital cost of each component at the foregoing optimum points. The main share of the capital cost is accounted for the MCFC stack which in all three operating points (single-objective I, II, and multi-objective opti-mization) encompasses more than 75% of the total capital cost. On the other hand, the noticeable voltage loss of the stack with time due to the degradation of the metal components, electrolyte vaporization, and dissolution of the cathode necessitates the user to also take into account the extra cost of stack replacement and/or reparation. Furthermore, the next highest capital cost is associated with the gas turbine and among the components of the ORC cycle the evaporator is the most expensive component. As can be observed in Table 8, the total cost rate of the optimum point selected by TOPSIS lies between that of the two extremes (point A and B). In point A in which the exergetic efficiency is most weighted, the total cost rate reaches its highest value, 0.01106 € s^{-1}; while in point B, the system is optimized only from economic point of view which leads to the lowest total cost rate, 0.00971 € s^{-1}, as well as the least exergetic efficiency of 49.44%. These two extreme scenarios which suffer from high total cost rate (Case A) and low exergetic efficiency (Case B) clearly point out the key role of the multi-objective optimization in bringing the balance and targeting the operating points with the best trade-off between the selected objectives. As a result, it can be noticed that both the exergetic efficiency and total cost rate of the TOPSIS selected point are in between of the limits obtained from the two extremes. In addition, Table 9 summarizes the amount of pollutant emissions and the corresponding environmental costs in each of the three optimization method. Expectedly, the least social cost of air pollution with the value of 6825 € per year is in Case A where the exergetic efficiency is the most weighted objective function; while this value increases by 3% in Case B and reaches 7015 € per year. This is due to the fact that higher exergetic efficiency leads to a more efficient operation with lower fuel consumption and consequently lower emissions.

10.3. Sensitivity analysis

As the fuel unit price is always subjected to change over time, investigating the effect of the variation of this parameter on the optimum solutions of the system would provide a better understanding in the behavior of the proposed plant. As such, Fig. 6 depicts the sensitivity of the Pareto optimum solutions to the variation of unit cost of fuel, i.e. 0.0092 € MJ^{-1} as the base value, as well as 0.0115 and 0.0069 € MJ^{-1} respectively. It can be seen in this figure, increasing the unit cost of fuel, the Pareto optimal solutions shift upward and leftward (with higher exergetic efficiency) simulta-neously. As a consequence of increasing the unit cost of fuel, the operating cost of the plant, which is included in the total cost rate, will rise which subsequently leads to the observed upward move-ment of the Pareto front. Moreover, it can be understood from the Pareto front shapes that the variation of the objective function is less sensitive to fuel cost at high exergetic efficiencies. Accordingly, in regions with high exergetic efficiency and low weight of ther-moenvironomic objective the Pareto front curves for different fuel costs converge. Further to the unit cost of fuel, the sensitivity of the Pareto optimum solution to the interest as another economic parameter has been performed. Fig. 7 illustrates the trends of Pareto front curve in case of interest rate of 1.2%, as the base value, and 3% as the extreme value. It can be noticed that the Pareto front solution has a similar behavior with interest rate variation as in case of fuel cost. Finally, Table 10 provides the results of sensitivity analysis of change in the numerical values of TOPSIS selected optimal design

Table 8
The performance-related results of the hybrid system from three optimization standpoints.

Parameter	Point A as an extreme in favor of exergetic efficiency	Point B as an extreme in favor of total cost rate	Multi objective optimization (trade-off approach)
Gas Turbine electrical power (kW)	89.85	86.1	92.4
MCFC electrical power (kW)	108.6	88.7	96.8
Air Compressor electrical power (kW)	48.82	48.74	48.6
ORC net electrical power (kW)	3.9	3.42	3.6
ORC exergetic efficiency (%)	45.8	42.8	44.3
MCFC exergetic efficiency (%)	38.4	30.8	35.6
Total exergetic efficiency (%)	56.06	49.44	54.95
Total cost rate (Euro/sec)	0.01106	0.00971	0.01023
Total annual cost (Euro)	318,528	279,648	294,624

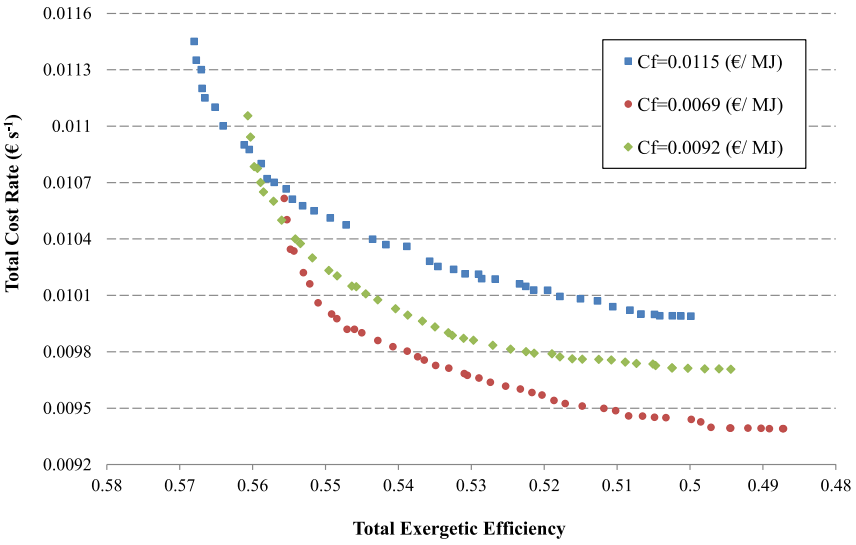

Fig. 6. The sensitivity of Pareto optimum solutions to the fuel unit cost.

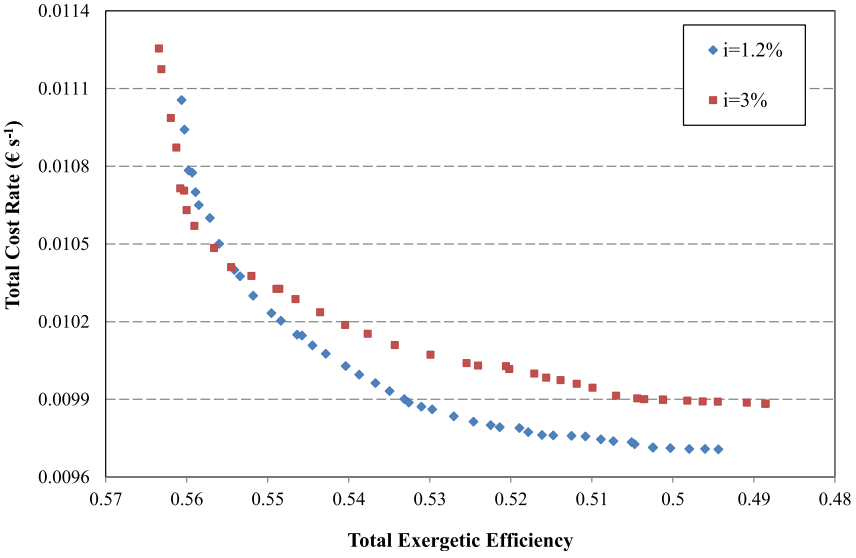

Fig. 7. The sensitivity of Pareto optimum solutions to the interest rate.

Table 10
The sensitivity analysis of change in the numerical values of optimum design parameters with variation in fuel unit cost.

Change in the values of design parameters	Variation in fuel unit cost	
	−25%	+25%
$\frac{\Delta TIT}{TIT}$	−1.95%	+2.16%
$\frac{\Delta r_c}{r_c}$	−4.42%	+5.85%
$\frac{\Delta \eta_T}{\eta_T}$	−0.38%	+0.41%
$\frac{\Delta U_f}{U_f}$	−2.23%	+2.57%
$\frac{\Delta (S/C)}{(S/C)}$	+2.41%	−2.78%
$\frac{\Delta T_{eva}}{T_{eva}}$	+2.35%	−1.82%
$\frac{\Delta dT_{pp-eva}}{dT_{pp-eva}}$	+3.88%	−4.13%
$\frac{\Delta T_{con}}{T_{con}}$	+2.15%	−2.68%
$\frac{\Delta dT_{pp-con}}{dT_{pp-con}}$	+1.18%	−3.42%

parameters with variation in the unit cost of fuel. As shown in Table 10, increasing the unit cost of fuel encourages the optimal design parameters shift to more thermodynamically efficient design.

11. Conclusions

In the present study, an MCFC-GT plant integrated with an ORC (organic Rankine cycle) was modeled for power production and analyzed from energetic, exergetic, economic, and environmental aspects (4E analysis). Employing the genetic algorithm optimization technique, multi-objective optimization of the system was conducted and the Pareto front optimum solutions were obtained. The objective functions in the system optimization were the total exergetic efficiency and the total cost rate (including the capital investment cost, operational cost, and environmental cost). The optimization results revealed that the multi-objective optimization approach, besides keeping the exergetic efficiency at high

levels, attempts to reach the minimum total cost rate of the system. The exergetic analysis of the MCFC-GT-ORC plant shows that there is at least a 5% gain in exergetic efficiency compared with the power cycle without any bottoming cycle. Finally, the sensitivity analysis of the variation of optimal design parameters as well as Pareto optimal solutions with alterations in the economic parameters (fuel unit cost and interest rate) was carried out and the results revealed that a 25% growth in the fuel unit cost increases the total cost rate by 3% in the low exergetic efficiency zone. On the other hand, it was observed that by increasing the interest rate the Pareto front curve shifts to regions with higher exergetic efficiency and total cost rate.

References

[1] Schenone C, Borelli D. Experimental and numerical analysis of gas distribution in molten carbonate fuel cells. Appl Enery 2014;122(0):216–36.

[2] Chacartegui R, Blanco MJ, Muñoz de Escalona JM, Sánchez D, Sánchez T. Performance assessment of molten carbonate fuel cell–humid air turbine hybrid systems. Appl Enery 2013;102(0):687–99.

[3] Najafi B, Haghighat Mamaghani A, Baricci A, Rinaldi F, Casalegno A. Mathematical modelling and parametric study on a 30 kWel high temperature PEM fuel cell based residential micro cogeneration plant. Int J Hydrogen Energy.(0).

[4] Wee J-H. Molten carbonate fuel cell and gas turbine hybrid systems as distributed energy resources. Appl Enery 2011;88(12):4252–63.

[5] Brouwer J, Jabbari F, Leal EM, Orr T. Analysis of a molten carbonate fuel cell: numerical modeling and experimental validation. J Power Sources 2006;158(1):213–24.

[6] Nguyen HVP, Song SA, Park D-N, Ham HC, Han J, Yoon SP, et al. Improved molten carbonate fuel cell performance via reinforced thin anode. Int J Hydrog Energy 2012;37(21):16161–7.

[7] Milewski J, Wołowicz M, Miller A, Bernat R. A reduced order model of molten carbonate fuel cell: a proposal. Int J Hydrog Energy 2013;38(26):11565–75.

[8] Sciacovelli A, Verda V. Sensitivity analysis applied to the multi-objective optimization of a MCFC hybrid plant. Energy Conv Manag 2012;60(0):180–7.

[9] Zhang X, Guo J, Chen J. Influence of multiple irreversible losses on the performance of a molten carbonate fuel cell-gas turbine hybrid system. Int J Hydrog Energy 2012;37(10):8664–71.

[10] Sánchez D, Muñoz de Escalona JM, Monje B, Chacartegui R, Sánchez T. Preliminary analysis of compound systems based on high temperature fuel cell, gas turbine and organic rankine cycle. J Power Sources 2011;196(9):4355–63.

[11] Bischoff M, Huppmann G. Operating experience with a 250 kWel molten carbonate fuel cell (MCFC) power plant. J Power Sources 2002;105(2):216–21.

[12] Liu A, Weng Y. Modeling of molten carbonate fuel cell based on the volume–resistance characteristics and experimental analysis. J Power Sources 2010;195(7):1872–9.

[13] Verda V, Sciacovelli A. Design improvement of circular molten carbonate fuel cell stack through CFD analysis. Appl Therm Eng 2011;31(14–15):2740–8.

[14] Kim H, Bae J, Choi D. An analysis for a molten carbonate fuel cell of complex geometry using three-dimensional transport equations with electrochemical reactions. Int J Hydrog Energy 2013;38(11):4782–91.

[15] Koh J-H, Kang BS, Lim HC. Analysis of temperature and pressure fields in molten carbonate fuel cell stacks. AIChE J 2001;47(9):1941–56.

[16] Desideri U, Proietti S, Sdringola P, Cinti G, Curbis F. MCFC-based CO_2 capture system for small scale CHP plants. Int J Hydrog Energy 2012;37(24):19295–303.

[17] Zhao Y, Chen J. Modeling and optimization of a typical fuel cell–heat engine hybrid system and its parametric design criteria. J Power Sources 2009;186(1):96–103.

[18] Lunghi P, Bove R, Desideri U. Analysis and optimization of hybrid MCFC gas turbines plants. J Power Sources 2003;118(1–2):108–17.

[19] Ubertini S, Lunghi P. Assessment of an ambient pressure MCFC: external heated GT hybrid plant with steam injection and post-combustion. Fuel Cells 2001;1(3–4):174–80.

[20] Varbanov P, Klemeš J, Shah RK, Shihn H. Power cycle Integration and efficiency increase of molten carbonate fuel cell systems. J Fuel Cell Sci Tech 2005;3(4):375–83.

[21] Pierobon L, Rokni M, Larsen U, Haglind F. Thermodynamic analysis of an integrated gasification solid oxide fuel cell plant combined with an organic Rankine cycle. Renew Energy 2013;60(0):226–34.

[22] Yan Z, Zhao P, Wang J, Dai Y. Thermodynamic analysis of an SOFC–GT–ORC integrated power system with liquefied natural gas as heat sink. Int J Hydrog Energy 2013;38(8):3352–63.

[23] Akkaya AV, Sahin B. A study on performance of solid oxide fuel cell-organic Rankine cycle combined system. Int J Energy Res 2009;33(6):553–64.

[24] Al-Sulaiman FA, Dincer I, Hamdullahpur F. Energy analysis of a trigeneration plant based on solid oxide fuel cell and organic Rankine cycle. Int J Hydrog Energy 2010;35(10):5104–13.

[25] Chan SH, Low CF, Ding OL. Energy and exergy analysis of simple solid-oxide fuel-cell power systems. J Power Sources 2002;103(2):188–200.

[26] Rashidi R, Dincer I, Berg P. Energy and exergy analyses of a hybrid molten carbonate fuel cell system. J Power Sources 2008;185(2):1107–14.

[27] Shirazi A, Aminyavari M, Najafi B, Rinaldi F, Razaghi M. Thermal–economic–environmental analysis and multi-objective optimization of an internal-reforming solid oxide fuel cell–gas turbine hybrid system. Int J Hydrog Energy 2012;37(24):19111–24.

[28] Silveira JL, Martins Leal E, Ragonha Jr LF. Analysis of a molten carbonate fuel cell: cogeneration to produce electricity and cold water. Energy 2001;26(10):891–904.

[29] Verda V, Nicolin F. Thermodynamic and economic optimization of a MCFC-based hybrid system for the combined production of electricity and hydrogen. Int J Hydrog Energy 2010;35(2):794–806.

[30] Ghirardo F, Santin M, Traverso A, Massardo A. Heat recovery options for on-board fuel cell systems. Int J Hydrog Energy 2011;36(13):8134–42.

[31] Monaco A, Di Matteo U. Life cycle analysis and cost of a molten carbonate fuel cell prototype. Int J Hydrog Energy 2011;36(13):8103–11.

[32] Sánchez D, Monje B, Chacartegui R, Campanari S. Potential of molten carbonate fuel cells to enhance the performance of CHP plants in sewage treatment facilities. Int J Hydrog Energy 2013;38(1):394–405.

[33] Xu J, Froment GF. Methane steam reforming, methanation and water-gas shift: I. Intrinsic kinetics. AIChE J 1989;35(1):88–96.

[34] Baranak M, Atakül H. A basic model for analysis of molten carbonate fuel cell behavior. J Power Sources 2007;172(2):831–9.

[35] Morita H, Komoda M, Mugikura Y, Izaki Y, Watanabe T, Masuda Y, et al. Performance analysis of molten carbonate fuel cell using a Li/Na electrolyte. J Power Sources 2002;112(2):509–18.

[36] Quoilin S, Declaye S, Tchanche BF, Lemort V. Thermo-economic optimization of waste heat recovery Organic Rankine Cycles. Appl Therm Eng 2011;31(14–15):2885–93.

[37] Chacartegui R, Sánchez D, Muñoz JM, Sánchez T. Alternative ORC bottoming cycles for combined cycle power plants. Appl Enery 2009;86(10):2162–70.

[38] Bao J, Zhao L. A review of working fluid and expander selections for organic Rankine cycle. Renew Sus Energy Rev 2013;24(0):325–42.

[39] Zhang HG, Wang EH, Fan BY. Heat transfer analysis of a finned-tube evaporator for engine exhaust heat recovery. Energy Conv Manag 2013;65(0):438–47.

[40] Kakaç S, Liu H, Pramuanjaroenkij A. Heat exchangers: selection, rating, and thermal design. 2nd ed. Taylor & Francis; 2002.

[41] Huang XY, Wang H, Wang HT. Experimental study on evaporating heat transfer characteristics of HFC-245fa. Wuhan Ligong Daxue Xuebao/J Wuhan Univ Technol 2011;33(3):67–71.

[42] Bertsch SS, Groll EA, Garimella SV. A composite heat transfer correlation for saturated flow boiling in small channels. Int J Heat Mass Transf 2009;52(7–8):2110–8.

[43] Ghiaasiaan SM. Two-phase flow, boiling, and condensation. In: Conventional and Miniature systems. Cambridge University Press; 2007.

[44] Najafi B, Shirazi A, Aminyavari M, Rinaldi F, Taylor RA. Exergetic, economic and environmental analyses and multi-objective optimization of an SOFC-gas turbine hybrid cycle coupled with an MSF desalination system. Desalination 2014;334(1):46–59.

[45] Najafi B, Najafi H, Idalik M. Computational fluid dynamics investigation and multi-objective optimization of an engine air-cooling system using genetic algorithm. Proc Institution Mech Eng Part C J Mech Eng Sci 2011;225(6):1389–98.

[46] Rizk NK, Mongia HC. Semianalytical correlations for NOx, CO, and UHC emissions. J Eng Gas Turbines Power 1993;115(3):612–9.

[47] Shirazi A, Najafi B, Aminyavari M, Rinaldi F, Taylor RA. Thermal–economic–environmental analysis and multi-objective optimization of an ice thermal energy storage system for gas turbine cycle inlet air cooling. Energy 2014;69:212–26.

[48] Aminyavari M, Najafi B, Shirazi A, Rinaldi F. Exergetic, economic and environmental (3E) analyses, and multi-objective optimization of a CO_2/NH_3 cascade refrigeration system. Appl Therm Eng 2014;65(1):42–50.

[49] Sayyaadi H. Multi-objective approach in thermoenvironomic optimization of a benchmark cogeneration system. Appl Energy 2009;86(6):867–79.

[50] Sanaye S, Katebi A. 4E analysis and multi objective optimization of a micro gas turbine and solid oxide fuel cell hybrid combined heat and power system. J Power Sources 2014;247(0):294–306.